PNAS RESEARCH ARTICLE | CELL BIOLOGY

Neutral sphingomyelinase 2 is required for HIV-1 maturation

Abdul A. Waheed[a,1], Yanan Zhu[b], Eva Agostino[a], Lwar Naing[a], Yuta Hikichi[a], Ferri Soheilian[c], Seung-Wan Yoo[d], Yun Song[e], Peijun Zhang[b,e,f], Barbara S. Slusher[d,g,h], Norman J. Haughey[d,h,1], and Eric O. Freed[a,1]

Edited by Stephen Goff, Columbia University Irving Medical Center, New York, NY; received November 18, 2022; accepted April 11, 2023

HIV-1 assembly occurs at the inner leaflet of the plasma membrane (PM) in highly ordered membrane microdomains. The size and stability of membrane microdomains is regulated by activity of the sphingomyelin hydrolase neutral sphingomyelinase 2 (nSMase2) that is localized primarily to the inner leaflet of the PM. In this study, we demonstrate that pharmacological inhibition or depletion of nSMase2 in HIV-1-producer cells results in a block in the processing of the major viral structural polyprotein Gag and the production of morphologically aberrant, immature HIV-1 particles with severely impaired infectivity. We find that disruption of nSMase2 also severely inhibits the maturation and infectivity of other primate lentiviruses HIV-2 and simian immunodeficiency virus, has a modest or no effect on nonprimate lentiviruses equine infectious anemia virus and feline immunodeficiency virus, and has no effect on the gammaretrovirus murine leukemia virus. These studies demonstrate a key role for nSMase2 in HIV-1 particle morphogenesis and maturation.

HIV-1 | nSMase2 | Gag processing | maturation | infectivity

HIV-1 assembly is driven by the viral Gag precursor protein Pr55Gag (hereafter referred to as Gag). Gag contains several structural and functional domains that serve specific functions during virus assembly and release: The matrix (MA) domain directs the binding of Gag to the inner leaflet of the plasma membrane (PM) and is also responsible for the incorporation of the viral envelope (Env) glycoproteins into virus particles; capsid (CA) is the key determinant of protein–protein interactions that drive particle assembly; nucleocapsid (NC) binds viral genomic RNA, thereby mediating its encapsidation into the virus particle, and promoting efficient particle assembly; and p6 drives particle release by recruiting the cellular endosomal sorting complex required for transport apparatus and associated factors that catalyze the membrane scission reaction required for the pinching off of the virus particle from the PM [reviews (1–3)]. HIV-1 Gag also contains two spacer peptides, SP1 and SP2, located between CA/NC and NC/p6 domains, respectively. While expression of Gag is sufficient to drive the assembly and release of noninfectious virus-like particles (VLPs), the production of mature, infectious particles requires expression of the GagPol polyprotein precursor, Pr160GagPol (hereafter referred to as GagPol), which is generated via a low-frequency (–)1 ribosomal frameshifting event during Gag translation. The GagPol precursor, which coassembles with Gag in virus particles, contains the domains for the viral enzymes protease (PR), reverse transcriptase (RT), and integrase (IN).

Gag is synthesized in the cytosol and subsequently traffics to the inner leaflet of the PM where virus assembly takes place. The phospholipid phosphatidylinositol-(4, 5)-bisphosphate [PI(4, 5)P_2] plays a central role in the binding of Gag to the inner leaflet of the PM (4, 5) through direct interactions between PI(4, 5)P_2 and the MA domain of Gag (6, 7). After Gag–membrane association, the CA domain of Gag assembles into an immature hexameric lattice that contains gaps, allowing the lattice to form a roughly spherical shell (8). Because retroviral PRs function as obligate dimers, GagPol must dimerize in order for PR to first cleave itself from GagPol and then form the mature dimeric enzyme that cleaves Gag and GagPol precursors into their constituent domains, triggering particle maturation (for reviews, see refs. 9 and 10). A primary feature of lentiviral particle maturation is the formation of a condensed conical core composed of an outer layer of CA protein (referred to as the capsid) and containing the viral RNA genome and viral enzymes RT and IN. In contrast to the conical core formed by lentiviruses, other retroviruses, like murine leukemia virus (MLV), form a spherical/polyhedral CA core (11, 12). Regardless of the core morphology, proper core condensation is absolutely required for particle infectivity (13); for reviews, see refs. 2 and 14.

HIV-1 assembly has been shown to take place in specialized, highly ordered membrane microdomains, often referred to as "lipid rafts," that are enriched in cholesterol, sphingomyelin, and phospholipid species with saturated acyl chains [(15–18); for reviews see refs. 19 and 20]. Consistent with the hypothesis that HIV-1 assembly takes place in lipid rafts, the viral envelope is enriched in cholesterol and sphingomyelin relative to the producer

Significance

HIV-1 particles acquire their viral envelope from the plasma membrane when they bud from the surface of the infected cell. The role that virion lipid composition plays in particle assembly, budding, and maturation remains poorly defined. In this study, we found that inhibiting the cellular ceramide–generating enzyme neutral sphingomyelinase 2 (nSMase2) in the virus-producer cell elicits a profound defect in particle maturation and infectivity. Similar effects were seen with HIV-2 and simian immunodeficiency virus, whereas several other retroviruses were less affected, or unaffected, under the same conditions. These results demonstrate a previously undescribed role for nSMase2 in the maturation of primate lentiviruses and suggest the possibility of unique antiretroviral therapeutic strategies aimed at disrupting this enzyme.

Author contributions: A.A.W. designed research; A.A.W., Y.Z., E.A., L.N., F.S., and Y.S. performed research; Y.H., S.-W.Y., B.S.S., and N.J.H. contributed new reagents/analytic tools; A.A.W. and P.Z. analyzed data; P.Z. coordinated cryoET analysis; E.O.F. coordinated and supervised the project; and A.A.W. and E.O.F. wrote the paper.

Competing interest statement: B.S.S. and N.J.H. are listed as inventors in patent applications filed by Johns Hopkins Technology Ventures covering novel compositions and utilities of nSMase2 inhibitors, including PDDC. This arrangement has been reviewed and approved by the Johns Hopkins University in accordance with its conflict of interest policies.

This article is a PNAS Direct Submission.

[1]To whom correspondence may be addressed. Email: abdul.waheed@nih.gov, nhaughe1@jh.edu, or efreed@nih.gov.

This article contains supporting information online at https://www.pnas.org/lookup/suppl/doi:10.1073/pnas.2219475120/-/DCSupplemental.

Published July 5, 2023.

cell membrane, and HIV-1 particles display a high degree of lipid order that is similar to raft-like membrane domains (21–26). Although the lipid composition of retroviruses other than HIV-1 has not been extensively studied, published data indicate that the lipid envelopes of HIV-2, simian immunodeficiency virus (SIV-B670), and MLV are also enriched in cholesterol and sphingomyelin (22, 24). The lipid composition of the avian retrovirus Rous sarcoma virus has also been reported to be distinct from that of the PM of its host cell (27). The Gag proteins of several retroviruses, including HIV-1 (16, 17, 28–33), MLV (34), and HTLV-1 (35), have been shown to associate with detergent-resistant membranes, which serve as a biochemical surrogate for raft association. Depletion of cellular cholesterol impairs HIV-1 assembly by inhibiting the association of Gag with the PM (17, 36), and removing cholesterol from the viral envelope disrupts HIV-1 particle infectivity (37–39). Together, these results indicate that the specialized lipid composition of the PM at viral assembly sites, and the raft-like properties of the viral envelope, play a critical role in the replication of HIV-1 and perhaps other retroviruses. However, the relationship between lipid composition and retroviral assembly, release, and maturation remains poorly understood.

Sphingomyelin is converted to ceramide and phosphorylcholine through the action of a family of sphingomyelinases that are classified based on their pH optima (alkaline, acidic, and neutral) (for review, see ref. 40). Neutral sphingomyelinase 2 (nSMase2) is the most extensively studied sphingomyelinase and is primarily localized to the PM. Ceramides are a diverse family of bioactive lipids that have been reported to play key roles in a variety of cellular processes including proliferation, apoptosis, differentiation, adhesion, autophagy, and the formation of a subset of extracellular vesicles (EVs) (41, 42). Recruitment of nSMase2 to the PM has been reported to be promoted by its interaction with the PI(4,5)P_2-binding protein TNF receptor 1–associated protein FAN (the WD-repeat protein factor associated with nSMase) (43, 44).

Several previous studies investigated the role of ceramide in HIV-1 replication. Blumenthal and colleagues reported that increasing ceramide levels in target cells inhibited HIV-1 infection (45), and Barklis et al. showed that the knockdown of ceramide synthase 2, which catalyzes the synthesis of very-long-chain ceramides, did not affect HIV-1 assembly but reduced the infectivity of virus particles produced from the knockdown cells (46). This effect appeared to be exerted at the level of membrane fusion.

EVs and enveloped virus particles share several properties, including their raft-like lipid composition. Because of the reported role of ceramide and nSMase2 in EV biogenesis, we sought to investigate a potential role for this enzyme in the late stages of HIV-1 replication. Our results show that inhibiting the activity of nSMase2 in virus-producing cells results in severe defects of HIV-1 Gag processing and particle morphogenesis. We demonstrate that other primate lentiviruses also depend on nSMase2 for Gag processing and proper particle formation, whereas MLV is unaffected by nSMase2 disruption. These results, together with those reported in the companion paper (Yoo et al.), identify nSMase2 as a key regulator of HIV-1 particle formation and maturation.

Results

Disruption of nSMase2 Impairs HIV-1 Gag Processing. To examine whether nSMase2 plays a role in HIV-1 assembly, release, and maturation, we treated virus-producing cells with a dose escalation of the potent and selective nSMase2 inhibitor phenyl(R)-(1-(3-(3,4-dimethoxyphenyl)-2,6-dimethylimidazo[1,2-b]pyridazin-8-yl)pyrrolidin-3-yl)-carbamate (PDDC) (pIC50 = 6.57) (47) and monitored Gag processing and particle release by western blot with anti-HIV immunoglobulin (HIV-Ig). These experiments used 293T, HeLa, and the human T cell line SupT1 as the virus-producer cells (Fig. 1 *A*–*C*). PDDC produced a strong and dose-dependent inhibition of Gag processing as evidenced by accumulation of the Gag precursor protein Pr55Gag, the Gag-processing intermediates p49 and p41, and correspondingly reduced levels of mature p24 (CA) in cell and viral lysates. Probing cell and virus lysates with anti-p17 (MA) and anti-p7 (NC) antibodies confirmed the impaired Gag processing in the presence of PDDC (*SI Appendix*, Fig. S1 *A* and *B*). These defects in Gag processing were not observed in the presence of an inactive structural analog of PDDC (control, compound 5; pIC50 < 4) in which the imidazo[1,2-b]pyridazine ring was substituted with a triazolo pyrimidine (Fig. 1 *A*–*C*, control lane) (47). Similar results were observed with all cell lines tested, with the lab-adapted, subtype B HIV-1 strain NL4-3, and the primary, subtype C transmitted/founder virus K3016 (also known as CH185; ref. 48) (*SI Appendix*, Fig. S2). We also tested a structurally distinct small-molecule inhibitor of nSMase2, 2,6-Dimethoxy-4-(5-Phenyl-4-Thiophen-2-yl-1H-Imidazol-2-yl)-Phenol (DPTIP) and its inactive des-hydroxy analog JHU3398 (49). As with PDDC, DPTIP treatment of virus-producer cells caused a strong and dose-dependent inhibition of HIV-1 Gag processing and infectivity, whereas the inactive structural analog JHU3398 had no effect (*SI Appendix*, Fig. S3).

The data presented above demonstrate that inhibition of nSMase2 in virus-producing cells severely disrupts HIV-1 Gag processing. To confirm a role for nSMase2 in the late stages of the HIV-1 replication cycle, we knocked down expression of nSMase2 using a lentiviral-delivered siRNA in HeLa and 293T cells transfected with pNL4-3. The siRNA-encoding lentiviral vector used in this study and in the companion paper (Yoo et al.) targets four sequences in the nSMase2 (also known as SMPD3) gene (*SI Appendix*, Fig. S4). The nSMase2 knockdown efficiency was approximately 60% in 293T cells (Fig. 1*D*). Consistent with the data obtained with PDDC, knockdown of nSMase2 severely disrupted Gag processing. In cells transduced with scrambled siRNA, fully cleaved p24 (CA) protein was detected in both cell and viral lysates. In contrast, in nSMase2-depleted cells, p24 (CA) was not generated and the Gag precursor protein Pr55Gag accumulated (Fig. 1*E*). These results confirm that disruption of nSMase2 in virus-producer cells severely impairs HIV-1 Gag processing.

In an effort to map domains in Gag that are responsible for the effect of nSMase2 disruption on Gag processing, we used several Gag mutants: NL4-3/Fyn10delMA, in which the MA domain has been replaced by the 10 N-terminal residues of C-Fyn (6); NL4-3/ILp1p6, in which the NC domain has been replaced by an isoleucine zipper (IL) (50); and NL4-3/L1term, in which the p6 domain has been removed by replacing the first amino acid codon of p6 (Leu) with a termination codon (51) (*SI Appendix*, Fig. S5*A*). In cells transduced with the Gag deletion mutants, Gag processing was severely impaired by disruption of nSMase2 activity with PDDC (*SI Appendix*, Fig. S5*B*) or siRNA-mediated knockdown (*SI Appendix*, Fig. S5*C*) with all constructs tested. A scrambled siRNA did not affect Gag processing. These results indicate that the MA, NC, or p6 domains of Gag are not individually required for the inhibitory effect of nSMase2 disruption on HIV-1 Gag processing.

Disruption of nSMase2 in the Virus-Producer Cell Impairs GagPol Processing but Does Not Reduce the Efficiency of Virus Particle Production or GagPol Incorporation into Virions. To determine whether inhibition of nSMase2 affects the efficiency of virus particle production, we transfected 293T cells with a

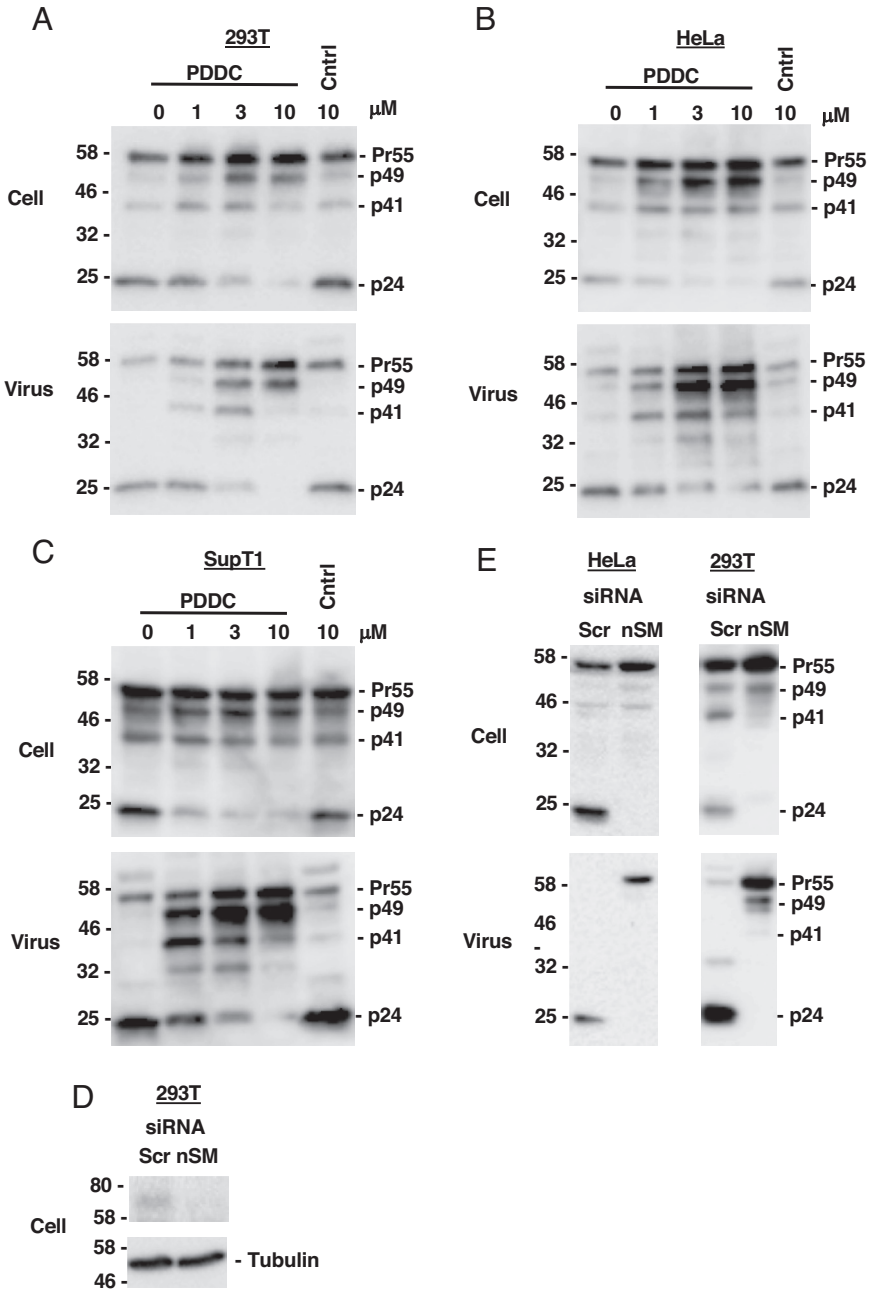

Fig. 1. Inhibition of nSMase2 activity impairs HIV-1 Gag processing. 293T (*A*) or HeLa (*B*) cells were transfected with the HIV-1 proviral clone pNL4-3 and 8 h posttransfection, cells were treated with the nSMase2 inhibitor PDDC at 0, 1, 3, and 10 μM or 10 μM inactive control compound 5 (Cntrl). After 24 h, cell and virus lysates were prepared and subjected to western blot analysis with HIV-Ig to detect the Gag precursor Pr55Gag (Pr55), Gag-processing intermediates (p49 and p41), and the CA protein p24. (*C*) SupT1 cells were transfected with pNL4-3 using DEAE-dextran. Six days posttransfection, the cells were divided into five equal parts, spun down, and the supernatant was replaced with medium containing 0, 1, 3, 10 μM PDDC or 10 μM control compound (Cntrl) and cultured for another 48 h. Cell and virus lysates were prepared and subjected to western blot analysis as in Fig. 1*A*. (*D* and *E*) HeLa or 293T cells were transduced with lentiviral particles carrying scrambled (Scr) or nSMase2 (nSM)-specific siRNA. One-day posttransduction, the cells were transfected with pNL4-3 and 24 h posttransfection, cell and virus lysates were prepared and subjected to western blot analysis as in Fig. 1*A*. nSMase2 knockdown efficiency was monitored by western blotting using an nSMase2-specific antibody (*D*). The mobility of molecular mass standards is shown on the left of each blot in kDa. Positions of the Gag precursor Pr55Gag (Pr55), Gag-processing intermediates (p49 and p41), and p24 (CA) are labeled on the right. A representative image from three independent experiments is shown.

PR-inactive derivative of pNL4-3, exposed cells to PDDC, and collected supernatants containing VLPs over time (2 to 24 h) for western blotting. Quantification of the blots indicated that PDDC did not substantially reduce the levels of VLP production at any time point tested (Fig. 2). Activity of PDDC in these assays was confirmed by treatment of cells expressing wild-type (WT) NL4-3; again, PDDC treatment severely impaired Gag processing.

To determine whether disruption of nSMase2 activity with either PDDC or nSMase2-specific siRNA impairs GagPol processing, or GagPol incorporation into virions, virus particles produced from cells treated with PDDC or nSMase2-specific siRNA and transfected with WT or PR(–) pNL4-3 (which contains a point mutation in the PR active site; ref. 51) were subjected to western blotting with HIV-Ig or anti-PR antiserum. Activity of PDDC and the nSMase2-specific siRNA was confirmed in this analysis by the accumulation of the Gag precursor and correspondingly reduced generation of the p24 (CA) protein (Fig. 3 *A* and *B*, NL4-3 lanes). In addition, disruption of nSMase2 activity or expression in the virus-producer cells resulted in the absence of virion-associated, mature PR (Fig. 3 *A* and *B*, *Lower*). However, disruption of nSMase2 had no effect on the levels of the GagPol precursor in PR(–) virus particles [Fig. 3 *A* and *B*, NL4-3/PR(–) lanes]. These results indicate that disruption of nSMase2 in virus-producer cells blocks not only Gag processing but also the processing of GagPol, resulting in a severe reduction in levels of mature PR in virus particles. The absence of PR in virions produced from nSMase2-disrupted cells is thus not the result of a defect in GagPol incorporation into virus particles.

The cytoplasmic tail of the MLV transmembrane Env protein p15(E) is cleaved during particle maturation by the viral PR to generate p12(E) (52, 53). We have shown that in HIV-1 particles pseudotyped with MLV Env, the HIV-1 PR will cleave the p15(E) cytoplasmic tail (54). p15(E) cleavage thus serves as an orthogonal approach to monitoring Gag processing for evaluating the activity

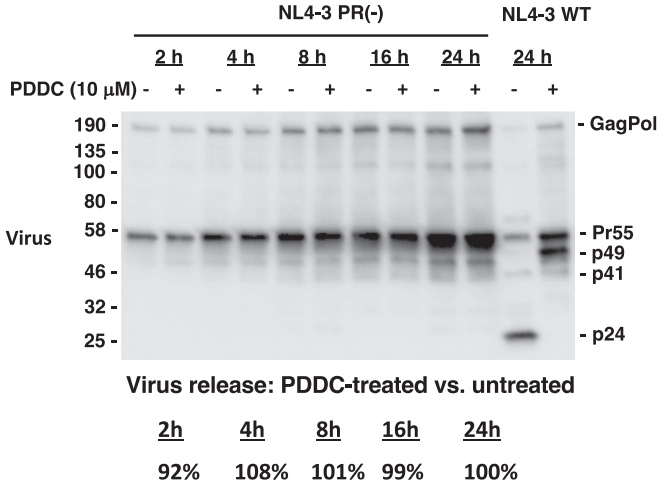

Fig. 2. PDDC does not affect the kinetics of HIV-1 particle release. 293T cells were transfected with pNL4-3 or the PR-defective derivative pNL4-3/PR(−) and 8 h posttransfection, cells were treated with 10 μM PDDC. Virus supernatants were collected after 2, 4, 8, 16, and 24 h and virus lysates were subjected to western blot analysis with HIV-Ig as in Fig. 1*A*. The mobility of molecular mass standards is shown on the left in kDa. The positions of the GagPol precursor Pr160GagPol, Pr55Gag (Pr55), p49, p41, and p24 (CA) are indicated on the right. The relative virus release of NL4-3/PR(−) from PDDC-treated cells compared to untreated cells based on the levels of particle-associated Pr55Gag at each time point averaged from two independent experiments is shown at the bottom. WT NL4-3 is shown in the last two lanes to demonstrate that PDDC is active in this assay.

of PR in HIV-1 particles. To examine whether nSMase2 disruption prevents PR-mediated cleavage of MLV p15(E), we pseudotyped Env(–) HIV-1 particles with amphotropic MLV Env (A-MLV Env) and measured the levels of p15(E) cleavage in the presence of PDDC or nSMase2 siRNA. The PR inhibitor amprenavir served as a positive control. Consistent with the reduced levels of mature PR in virions produced from nSMase2-disrupted cells (Fig. 3), we observed a loss of p15(E) cleavage to p12(E) in particles produced from cells treated with PDDC or nSMase2 siRNA (*SI Appendix*, Fig. S6). As expected, p15(E) cleavage was also blocked by the PR inhibitor amprenavir.

Disruption of nSMase2 in Virus-Producer Cells Inhibits HIV-1 Infectivity. As mentioned in the Introduction, Gag processing is required for virus maturation and subsequent infection. To determine the extent to which the Gag processing defect imposed by nSMase2 disruption impairs HIV-1 infectivity, the TZM-bl indicator cell line (55) was used to measure the infectivity of virus produced from 293T, HeLa, and SupT1 cells treated with PDDC. As shown in Fig. 4 *A*–*C*, we observed a dose-dependent inhibition of viral infectivity upon addition of PDDC, with a >100-fold reduction in infectivity at the highest dose of PDDC (10 μM) in all cell lines tested. As expected, the infectivity of virions produced in the presence of the inactive PDDC analog Cmpd-5 was not impaired. To corroborate the PDDC data, we examined whether depletion of nSMase2 with siRNA in virus-producer cells also reduces HIV-1 infectivity in TZM-bl cells. Virus stocks obtained from HeLa or 293T cells transduced with control-scrambled siRNA or nSMase2-specific siRNA were used to infect the TZM-bl indicator cell line. We observed a profound loss of infectivity of virus produced from cells treated with the nSMase2-specific siRNA relative to the scrambled siRNA (Fig. 4*D*). These data demonstrate that disruption of nSMase2 in virus-producer cells with either a pharmacological inhibitor or siRNA markedly impairs HIV-1 infectivity. This loss of infectivity was also seen with a primary, subtype C transmitted/founder virus (*SI Appendix*, Fig. S2*B*).

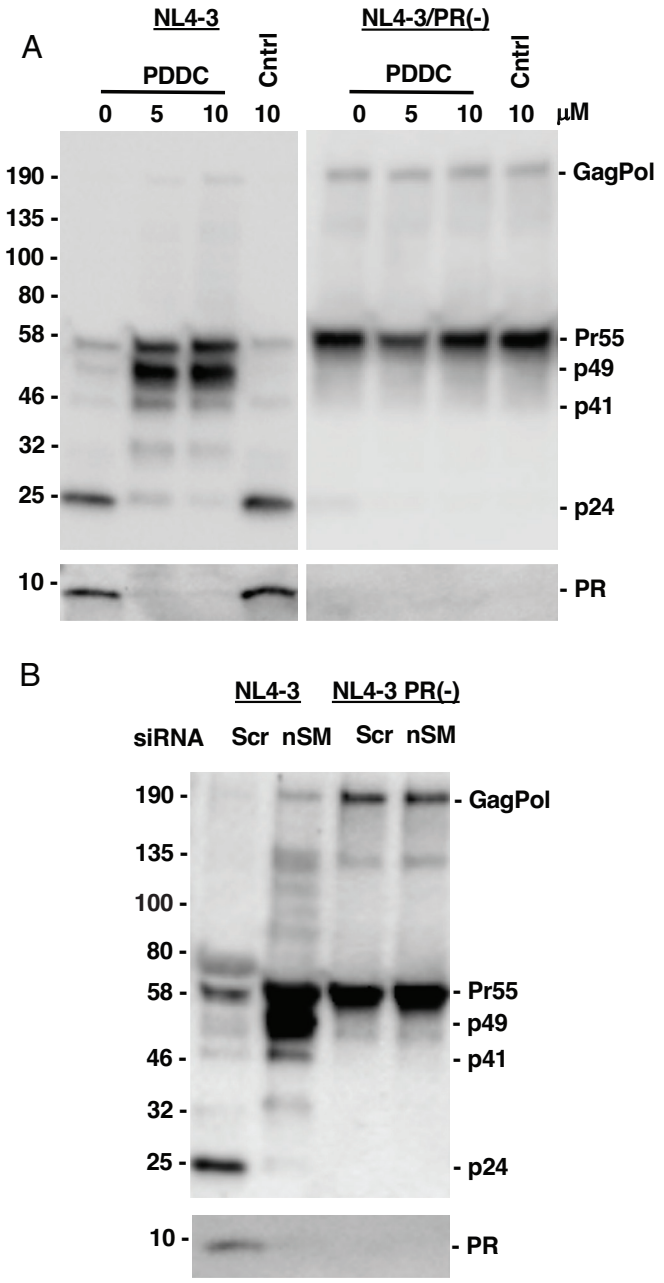

Fig. 3. The defect in Gag processing imposed by disruption of nSMase2 is not due to impaired GagPol incorporation into virions. (*A*) 293T cells were transfected with pNL4-3 or the PR-defective derivative pNL4-3/PR(−) and 8 h posttransfection, cells were treated with 0, 5, and 10 μM PDDC or 10 μM inactive control compound (Cntrl). Twenty-four hours posttransfection, cell and virus lysates were prepared and subjected to western blot analysis with HIV-Ig as in Fig. 1*A* or anti-HIV PR antibody. (*B*) 293T cells were transduced with lentiviral particles carrying scrambled (Scr) or nSMase2 (nSM)-specific siRNA as in Fig. 1*E* and 24 h posttransduction, cells were transfected with WT pNL4-3 or the PR-defective derivative pNL4-3/PR(−), and virus lysates were prepared and subjected to western blot analysis as in Fig. 3*A*. The mobility of molecular mass standards is shown on the left of each blot in kDa. The positions of GagPol, Pr55, p49, p41, p24, and PR are labeled on the right. A representative image from two independent experiments is shown.

Disruption of nSMase2 Activity with PDDC Impairs HIV-1 Replication in Spreading Infections. To determine whether PDDC treatment disrupts HIV-1 replication, the SupT1 T cell line was transfected with the full-length HIV-1 molecular clone pNL4-3. Transfected cells were treated with a dose escalation of PDDC, or were left untreated, and virus replication was monitored by measuring RT activity in the supernatant (Fig. 5*A*).

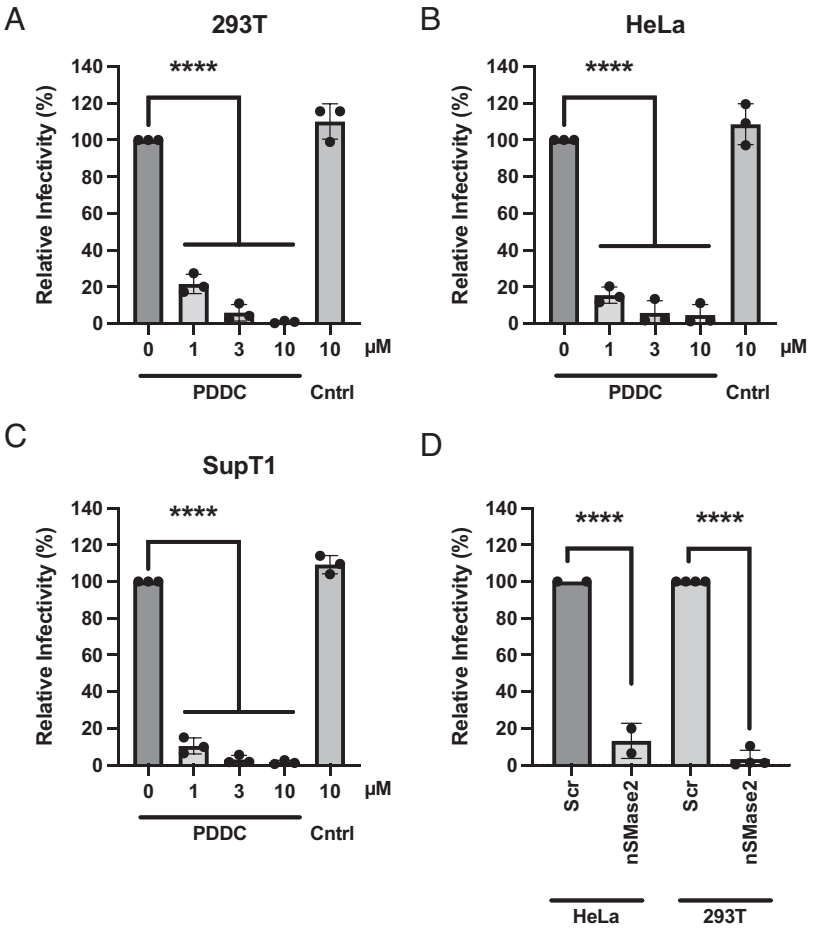

Fig. 4. Inhibition of nSMase2 activity in virus-producing cell impairs HIV-1 particle infectivity. 293T (*A*), HeLa (*B*), or SupT1 (*C*) cells were transfected with pNL-3 and treated with PDDC or control compound (Cntrl) as in Fig. 1 *A*–*C*. Six days posttransfection, SupT1 cells were divided equally, spun down, and then treated with PDDC or control compound (Cntrl) and cultured for another 48 h. Virus-containing supernatants were harvested and equal volumes were used to infect TZM-bl cells. Two days postinfection, luciferase activity was measured. The infectivity of HIV-1 in the absence of PDDC was set to 100%. (*D*) HeLa or 293T cells were transduced with lentiviral particles carrying scrambled (Scr) or nSMase2-specific siRNA; 24 h after transduction, cells were transfected with pNL4-3, and the virus-containing supernatants were harvested, and equal volumes were used to infect TZM-bl cells as in panels *A*–*C*. The infectivity of HIV-1 in the absence of PDDC was set to 100%. Data shown are ±SD from three independent experiments. ****$P < 0.0001$.

In the untreated SupT1 cells, HIV-1 replication peaked at around 10 d posttransfection. In the cultures treated with 0.1 μM PDDC, only a slight delay in virus replication was observed, whereas 1.0 μM PDDC completely blocked replication during the time frame of the experiment. At 0.3 μM, replication was delayed by several weeks relative to the untreated cultures (Fig. 5*A*). To determine whether PDDC blocked replication in primary peripheral blood mononuclear cells (PBMCs), cells from three different donors were infected with 293T-derived NL4-3 virus and RT activity was monitored over time in the presence or absence of PDDC. As observed in the SupT1 T cell line, concentrations of PDDC of 0.3 or 1.0 μM PDDC severely impaired or blocked HIV-1 replication (Fig. 5*B*). The IC_{50} concentration of PDDC for nSMase2 is 0.3 μM, and the concentration at which HIV-1 replication was blocked is in line with its potency for inhibition of nSMase2. These results demonstrate that the activity of nSMase2 is required for HIV-1 replication in both primary and immortalized T cells.

nSMase2 in Virus-Producer Cells Is Not Required for HIV-1 Env Incorporation. The results presented above demonstrate that inhibition of nSMase2 activity in virus-producer cells results in a severe defect in virus particle infectivity. To examine whether a defect in Env incorporation contributes to this loss of infectivity, we measured the levels of the surface Env glycoprotein gp120 and transmembrane Env glycoprotein gp41 in virions produced from cells treated with either PDDC (*SI Appendix*, Fig. S7*A*) or nSMase2-specific siRNA (*SI Appendix*, Fig. S7*B*). For this analysis, we used both WT [PR(+)] and PR(−) particles. We observed no consistent reduction in the levels of gp120 or gp41 in virus particles produced from cells treated with PDDC or nSMase2-specific siRNA (*SI Appendix*, Fig. S7 *A* and *B*), indicating that nSMase2 is not required for Env incorporation.

PDDC Treatment of Target Cells Does Not Impair HIV-1 Infectivity. Previous studies have demonstrated that depletion of cholesterol or increasing levels of ceramide in target cells has a significant impact on HIV-1 infectivity (39, 45, 56–59), suggesting that raft-like microdomains in the PM function in promoting HIV-1 infection. To investigate whether inhibiting nSMase2 activity in target cells has an effect on HIV-1 infectivity, we treated TZM-bl target cells with a dose escalation of PDDC and then infected with WT HIV-1. Luciferase activity was measured 2 d postinfection. We did not observe any reduction in HIV-1 infectivity even when target cells were treated with the highest concentration of PDDC for 48 h prior to infection (*SI Appendix*, Fig. S8). These results demonstrate that, under these conditions, nSMase2 in the target cell is not required for virus particle infectivity.

Disruption of nSMase2 Activity Impairs HIV-1 Particle Morphogenesis and Maturation. The defect in Gag processing and the subsequent loss of infectivity imposed by PDDC treatment and nSMase2 knockdown suggest that disruption of nSMase2 activity in virus-producer cells would likely be accompanied by aberrant virion maturation. We investigated this question by performing thin-section transmission electron microscopy (TEM). As expected, a high percentage of HIV-1 particles produced from untreated cells or cells treated with nontargeting siRNA exhibited a mature morphology characterized by the presence of condensed conical cores (Fig. 6 *A* and *C*, blue arrowheads). In contrast, virus

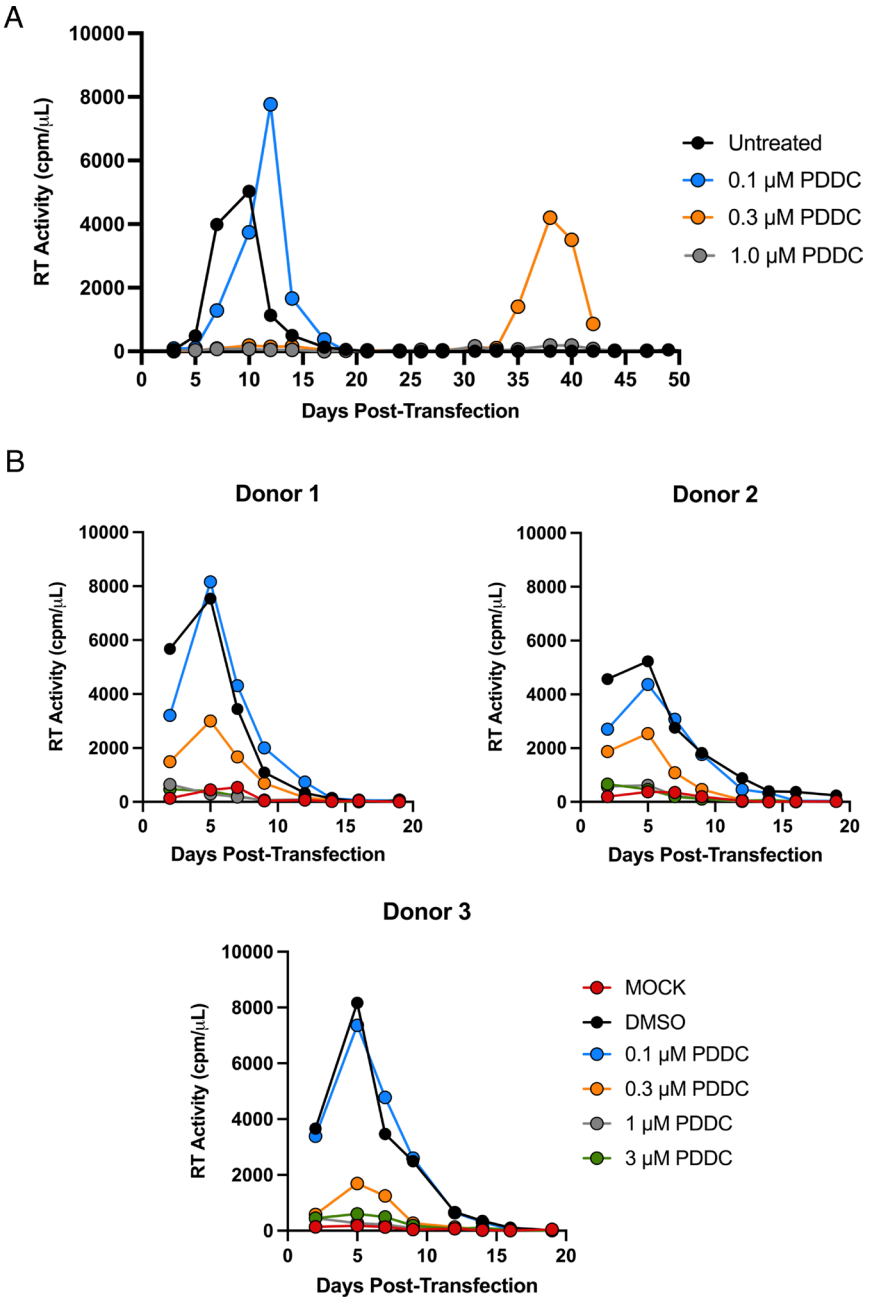

Fig. 5. PDDC blocks HIV-1 replication in T cells. (*A*) The SupT1 T cell line was transfected with the infectious HIV-1 molecular clone pNL4-3 and was cultured in the absence or presence of 0.1, 0.3, and 1 μM of PDDC. Cells were split every 2 or 3 d, and virus replication kinetics were monitored by measuring RT activity in the supernatant at each time point. The results are representative of at least two independent experiments. (*B*) 293T-derived NL4-3 virus stocks were used to infect PBMCs from three different donors (donors 1 to 3), and replication kinetics in the absence and presence of PDDC were monitored by measuring RT activity.

particles produced from nSMase2-depleted cells (Fig. 6*B*) or cells treated with 1 or 3 μM PDDC (Fig. 6 *D* and *E*) lacked conical cores and instead displayed a primarily immature morphology (orange arrowheads). In addition, many of the particles produced from nSMase2-disrupted cells showed a large gap in the Gag lattice (gray arrowheads) and a number contained blebs or "tails" (yellow arrowheads) (Fig. 6 *B*, *D*, and *E*). To quantify these ultrastructural phenotypes, we classified the virions into four subgroups: mature, immature, containing a large gap in the Gag lattice, and "tail" containing (Fig. 6 *F* and *G*). This scoring indicated that none of the HIV-1 particles from nSMase2-disrupted cells contained conical cores characteristic of mature virions. In contrast, the number of immature particles or particles containing large gaps in the Gag lattice or tails was markedly elevated in the context of either nSMase2 KD or PDDC treatment. Disruption of nSMase2 activity in virus-producer cells did not significantly affect the virus particle diameter, but many virions were oddly shaped (Fig. 6 *F* and *G*). These results indicate that nSMase2 disruption not only results in a severe defect in particle maturation (as would be predicted from the loss of Gag processing) but also produces other aberrant features. Even at concentrations of PDDC in the range of 0.2 to 0.4 μM, similar defects in virion morphogenesis were observed (*SI Appendix*, Fig. S9 *A–D*), although an occasional mature particle could be detected at these concentrations. These concentrations of PDDC also impaired Gag processing (*SI Appendix*, Fig. S9*E*). This is consistent with the replication data presented above showing that 0.3 μM PDDC significantly delays virus replication.

To examine the effect of PDDC on the morphology of HIV-1 particles produced from a T cell line, virions produced from SupT1 cells infected with NL4-3 were collected by ultracentrifugation and examined by TEM. The results were consistent with those obtained in 293T and Hela cells; most of the particles from untreated cells exhibited a mature morphology with condensed, conical cores (*SI Appendix*, Fig. S10 *A* and *D*; blue arrowheads), whereas many particles obtained from PDDC-treated cells contained a large gap in the Gag lattice (*SI Appendix*, Fig. S10 *B–D*, orange arrowhead),

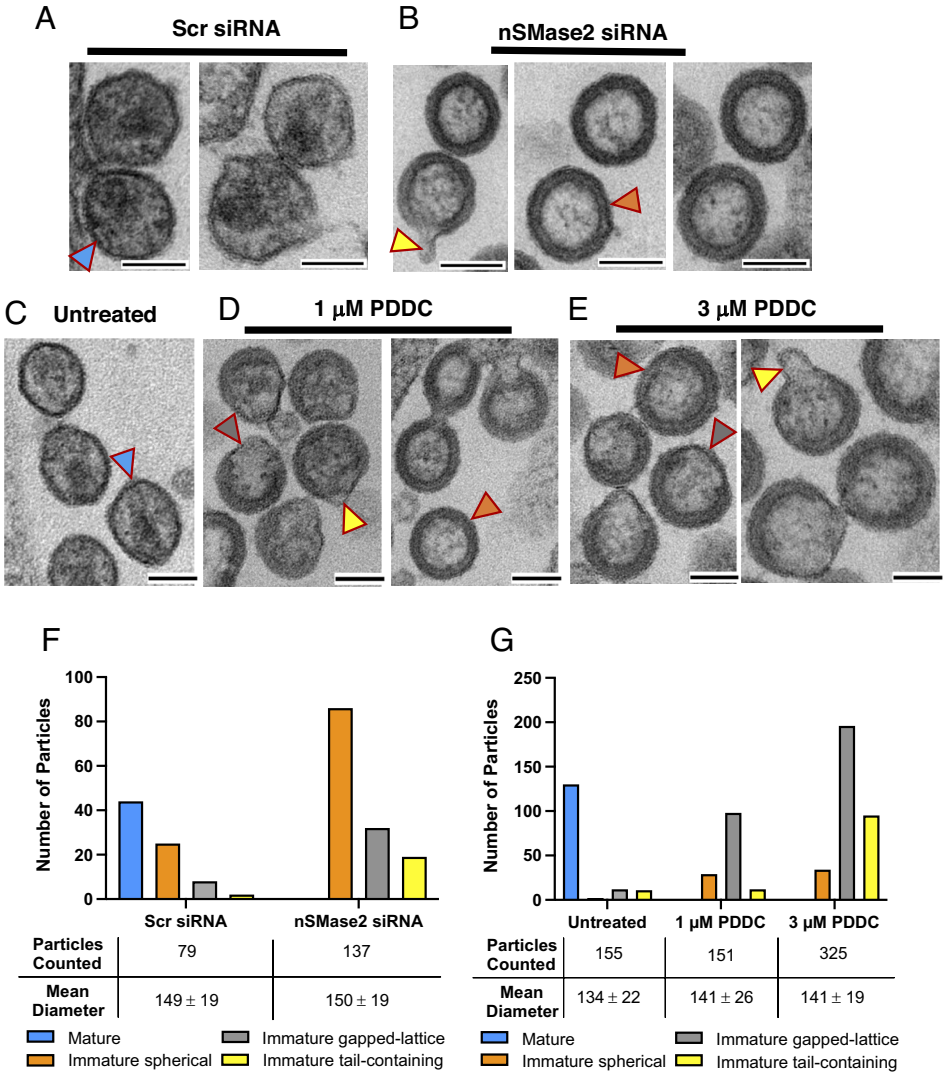

Fig. 6. Disrupting nSMase2 activity in virus-producer cells alters the morphology of HIV-1 particles. (*A* and *B*) 293T cells were transduced with lentiviral particles carrying scrambled (Scr) (*A*) or nSMase2-specific (*B*) siRNA and 1 d later were transfected with pNL4-3 as in Fig. 1*E*. One day posttransfection, cells were fixed in 2.5% glutaraldehyde and analyzed by thin-section EM. (*C*–*E*) pNL4-3-transfected 293T cells were either untreated (*C*) or treated with 1 μM (*D*) or 3 μM (*E*) PDDC for 24 h and processed for EM as in panels *A* and *B*. The following virion morphologies are highlighted: mature (blue arrowhead), immature spherical (orange arrowhead), immature with a large gap in the Gag lattice [gapped-lattice (gray arrowhead)], and immature "tail" containing (yellow arrowhead). (*F* and *G*) Quantification of virion morphology produced from 293T cells transduced with nontargeting or nSMase2-specific siRNA (*F*), and untreated or PDDC-treated 293T cells (*G*). The number of particles counted in each group and the mean diameter of the particles are indicated at the bottom of the bar diagram. (Scale bars represent 100 nm.)

and membrane blebs or tails (*SI Appendix*, Fig. S10 *B*–*D*, grey arrowhead). Overall, these data demonstrate that nSMase2 plays a critical role in HIV-1 morphogenesis independent of producer cell type. The production of oddly shaped virions with tails and large gaps in the Gag lattice that occurs when nSMase2 activity or expression is reduced is a likely result of altered lipid composition in the virion (see Yoo et al. companion paper for additional data).

To investigate further the effect of nSMase2 disruption on HIV-1 virion morphogenesis, we carried out cryo-electron tomography (cryo-ET) of immature VLPs in the presence and absence of PDDC. Interestingly, compared with the VLPs in the untreated sample (Fig. 7*A* and Movie S1), the three dimensional (3D) tomograms indicated that many (~36%) of the PDDC-treated VLPs show sizable indentations (Fig. 7 *B*-*E*) with infrequent protrusions (Movie S2). Despite these morphological aberrations, PDDC treatment did not change the average diameter of VLPs in the 3D tomograms (Fig. 7*F*), consistent with the TEM data presented above. To determine whether PDDC treatment alters the structure of the immature Gag lattice, we conducted cryo-ET subtomogram averaging (STA) using emClarity (60). The Gag structures were determined to 3.7 and 4.3 Å resolutions for untreated and PDDC-treated particles, respectively (*SI Appendix*, Figs. S11 *A* and *B* and S12 and Table S1). The structural elements of the immature Gag lattice, including the presence of the small polyanionic host assembly cofactor inositol hexakisphosphate (IP6) (61), were well resolved. An overlay of the structures from untreated and PDDC-treated VLPs shows their high degree of structural similarity (*SI Appendix*, Fig. S11*C*), indicating that PDDC treatment does not substantially alter Gag folding. We further analyzed the Gag immature lattice from untreated and PDDC-treated VLPs. As illustrated in *SI Appendix*, Fig. S11*D*, the overall hexagonal Gag lattices are similar between PDDC-treated and untreated VLPs, and both surface lattices are incomplete with holes.

nSMase2 Activity Is Required for Gag Processing and Particle Morphogenesis of Some, but Not Other, Retroviruses. The results presented thus far have focused on the effect of nSMase2 disruption on HIV-1 Gag and GagPol processing, maturation, and infectivity. Next, we sought to investigate the effect on Gag processing and maturation in the context of other retroviruses. We selected two closely related primate lentiviruses, SIVmac and HIV-2, two nonprimate lentiviruses Equine Infectious Anemia Virus (EIAV) and Feline immunodeficiency virus (FIV), and the gammaretrovirus MLV. We included HIV-1 in these experiments as a positive control. Virus particles were produced in 293T or CrFK (FIV) cells in the presence of 5 or 10 μM PDDC or 10 μM inactive control compound. Similar to HIV-1, treatment of virus-producer cells with PDDC disrupted SIVmac and HIV-2 Gag processing, as indicated by reduced levels of virion-associated CA and accumulation of Gag-processing intermediates (Fig. 8 *A*–*C*). EIAV

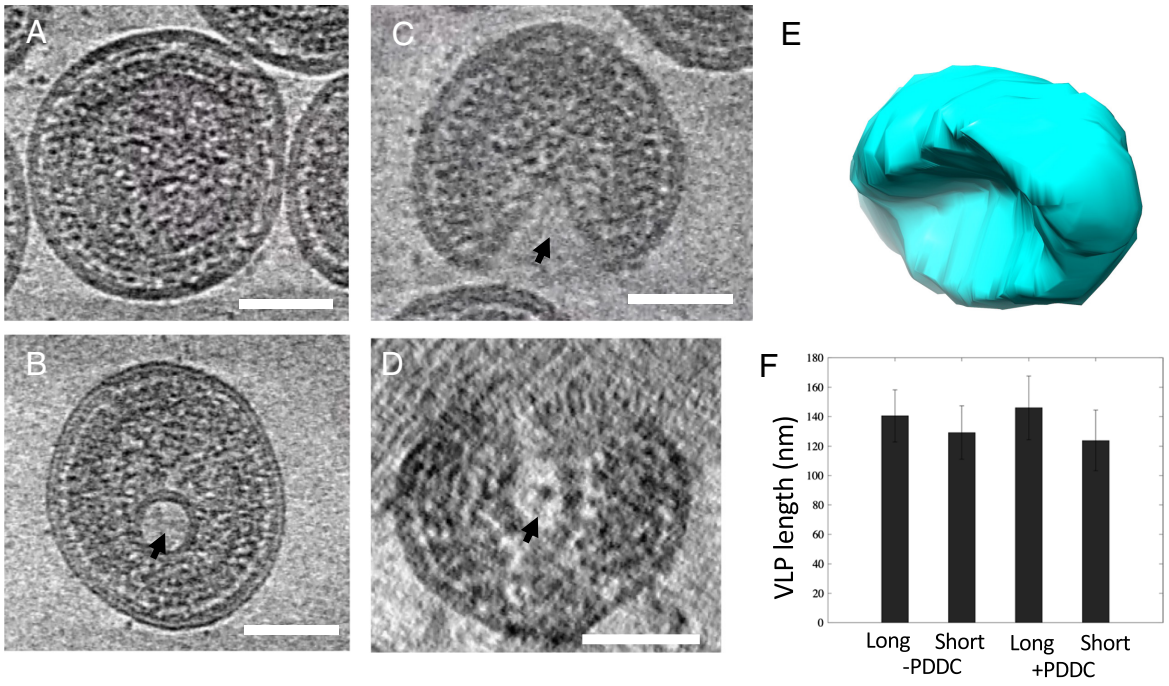

Fig. 7. Cryo-ET and STA of PDDC-treated immature particles (*A*) Tomographic slice of an untreated VLP. (*B*) A tomographic slice of a PDDC-treated VLP displaying indentation, shown with a face-on view. (*C* and *D*) Tomographic slices of a PDDC-treated VLP are shown in side view (*C*) and a 90° rotated view (*D*). 36% of virions (55/152) exhibited an indentation. (*E*) Segmentation of the VLP surface is shown in (*C*) and (*D*). (*F*) Analysis of the size of VLPs with (105 VLPs) and without (99 VLPs) PDDC treatment. (Scale bars, 50 nm.)

also showed some increased levels of Gag-processing intermediates in the presence of PDDC, although levels of CA protein were not substantially altered (*SI Appendix*, Fig. S13*A*). In contrast, FIV and MLV Gag processing was not discernably affected by PDDC (*SI Appendix*, Fig. S13*B* and Fig. 8*D*). These results demonstrate variable effects across different retroviruses in the impact of nSMase2 disruption on Gag processing.

We next investigated the effect of PDDC treatment on the infectivity of a range of retroviruses. 293T cells were transfected with HIV-1, HIV-2, SIVmac, or MLV molecular clones; the cells were treated with varying concentrations of PDDC; and the infectivity of the released particles was measured. Consistent with the western blotting data shown in Fig. 8, the infectivity of HIV-1, SIVmac, and HIV-2 was markedly impaired by PDDC treatment (Fig. 8 *A*–*C*). In contrast, and consistent with the lack of an effect on MLV Gag processing, the infectivity of MLV particles was not reduced by PDDC treatment, even at the highest concentration tested (10 μM) (Fig. 8*D*).

Next, we examined the morphology of a subset of virions sensitive (SIVmac, HIV-2) or insensitive (FIV, MLV) to nSMase2 disruption by TEM. Consistent with the defect in Gag processing, and similar to HIV-1, the morphology of SIVmac and HIV-2 particles produced in the presence of PDDC was uniformly immature (orange arrowhead) and some virions contained tail-like structures (yellow arrowhead) or had large gaps in the Gag lattice (gray arrowheads) (*SI Appendix*, Fig. S14 *A* and *B*). These TEM morphologies are strikingly similar to those observed for HIV-1 following nSMase2 disruption. Unlike lentiviral particles, which contain conical cores, mature MLV virions contain a spherical/polyhedral CA core (11, 12). Consistent with the lack of an effect of nSMase2 disruption on FIV and MLV Gag processing and infectivity, FIV and MLV particles produced in the presence of PDDC were morphologically indistinguishable from particles produced from untreated cells (*SI Appendix*, Fig. S14 *C* and *D*). These results, together with the biochemical and infectivity data presented above, demonstrate that nSMase2 is required for the production of mature particles of some but not all retroviruses. We also knocked down the expression of nSMase2 in 293T cells and examined the effect on SIVmac, HIV-2, EIAV, and MLV Gag processing. Consistent with the Gag-processing defects observed with PDDC, knockdown of nSMase2 severely impaired the processing of SIVmac (*SI Appendix*, Fig. S15*A*) and HIV-2 (*SI Appendix*, Fig. S15*B*) Gag, modestly affected EIAV Gag processing (*SI Appendix*, Fig. S15*E*), but had no effect on MLV (*SI Appendix*, Fig. S15*F*). TEM analysis of SIVmac and HIV-2 produced from nSMase2-depleted cells showed immature virions (orange arrowhead) and some with large gaps in the Gag lattice (gray arrowheads) or tail-like structures (yellow arrowhead) (*SI Appendix*, Fig. S15 *C* and *D*). In contrast, nSMase2 knockdown had no discernible effect on the morphology of MLV particles (*SI Appendix*, Fig. S15*G*).

Discussion

In this study, we report that disruption of the sphingomyelin hydrolase nSMase2 in virus-producer cells elicits a variety of profound effects on the morphogenesis and maturation of HIV-1 particles. Gag and GagPol processing are severely inhibited in the presence of either the nSMase2 inhibitor PDDC or nSMase2-specific siRNA, resulting in a loss of particle infectivity and spreading replication. This defect is independent of cell type, as impaired Gag processing was observed in HeLa and 293T cells and in the SupT1 T cell line, and PDDC inhibited virus replication in SupT1 cells and primary PBMCs. These effects are also not HIV-1 isolate dependent, as similar effects on Gag processing and particle infectivity were observed with a lab-adapted subtype B strain and a primary subtype C transmitted/founder virus. HIV-1 virions produced from nSMase2-disrupted cells display unusual "blebs" or tails and large gaps in the immature Gag lattice. Cryo-ET analysis revealed that a substantial fraction of particles contain large

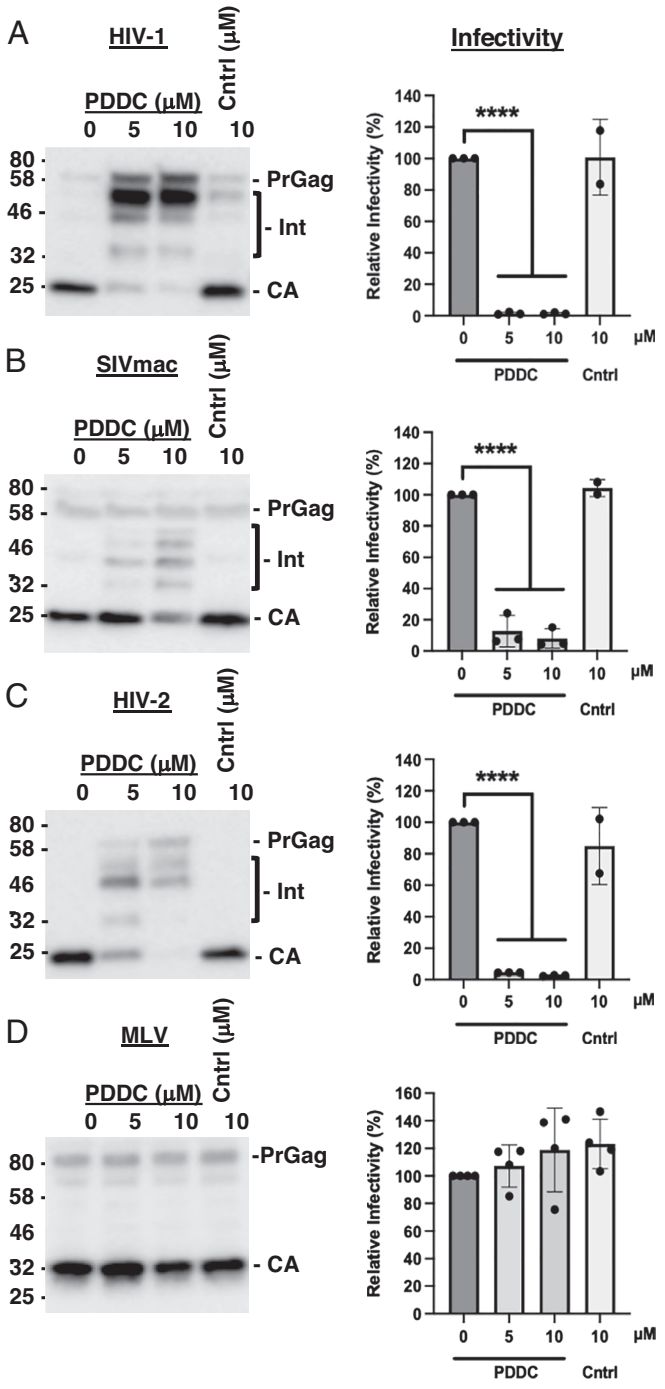

Fig. 8. PDDC inhibits SIVmac and HIV-2 Gag processing and particle infectivity but has no effect on MLV. 293T cells were transfected with plasmids expressing HIV-1, SIVmac, HIV-2, or MLV, and 8 h posttransfection, cells were treated with 0, 5, and 10 μM PDDC or 10 μM control compound (Cntrl). After 24 h, virus-containing supernatants were harvested, and a portion was retained for infectivity assay and the remainder was concentrated by ultracentrifugation. Cell and virus lysates were prepared and subjected to western blot analysis with HIV-Ig to detect HIV-1 (*A*), SIVmac (*B*), or HIV-2 (*C*) Gag proteins, and anti-MLV p30 (CA) to detect MLV Gag (*D*). (Right) TZM-bl cells were infected with equal volumes of HIV-1, SIVmac, and HIV-2 and 2 d postinfection, luciferase activity was measured as in Fig. 4. To monitor the effect of PDDC on MLV infectivity, 293T cells were cotransfected with the MLV molecular clone pRR390 and MLV-based luciferase-expressing clone pRR460 and treated with 0, 5, and 10 μM PDDC or control compound (Cntrl) as in Fig. 8*D*. Virus-containing supernatant was harvested, and equal volumes were used to infect HT1080 cells; 2 d later, luciferase activity was measured. The mobility of molecular mass standards is shown on the left of each blot in kDa. The positions of the Gag precursors (PrGag), Gag-processing intermediates (Int), and CA proteins are indicated on the right. A representative image from at least three independent experiments is shown. Infectivity in the absence of PDDC was set to 100%. Data shown are ± SD from three independent experiments. ****$P < 0.0001$.

indentations, consistent with membrane deformations at sites of Gag lattice discontinuity. Despite these morphological defects, cryo-ET and STA demonstrated that the local structure of the immature Gag lattice is not discernably altered by nSMase2 disruption. nSMase2 activity is not required for Env incorporation into virions, and treatment of target cells with PDDC does not impair particle infectivity. nSMase2 disruption in the virus-producer cell interferes with Gag processing and particle morphogenesis for HIV-2 and SIVmac, but has a milder or no effect on nonprimate lentiviruses FIV and EIAV and no effect on the gammaretrovirus MLV. These results identify nSMase2 as a key cellular factor in the maturation of primate lentiviruses.

Gag processing and subsequent particle maturation require the recruitment of the GagPol precursor into virus particles. Retroviral PRs function as obligate homodimers, with each monomer contributing half of the active site; GagPol dimerization is therefore essential to the initial proteolytic events (for review, see ref. 62). GagPol dimerization has been proposed to be driven by sequences in the RT and PR domains of GagPol (63) and GagPol dimers are less stable and less enzymatically active than mature PR dimers [(64, 65); see ref. 62 for review]. The inherently low activity of GagPol dimers is likely a mechanism to prevent premature PR activity before completion of particle assembly and release. Upon GagPol dimerization and PR activation, the PR domain cleaves itself from the GagPol precursor and is then able to cleave its target sites in Gag and GagPol, triggering particle maturation. PR activation is tightly regulated, as premature activation (e.g., by overexpressing GagPol relative to Gag) inhibits virus assembly (66–69) and delayed or impaired PR activity disrupts particle maturation and infectivity (70–74). Our data demonstrate that disruption of nSMase2 in virus-producer cells does not reduce the levels of virion-associated GagPol; the lower levels of PR in virions, and the block in Gag processing, may thus be the result of a defect in PR activation. The timing of PR activation relative to virus assembly and release has been addressed in several studies (75, 76) with recent data using a FRET-based reporter for PR activity suggesting that PR is activated in virus-producer cells and that proteolysis is completed very soon (seconds or minutes) after virus release (77). Because levels of Gag in virions exceed those of GagPol by a factor of ~20, each molecule of GagPol is surrounded by a large number of molecules of Gag. Dimerization of GagPol monomers may thus require conformational flexibility facilitated by specific properties of the viral membrane, and changes in the membrane composition of HIV-1 particles resulting from disruption of nSMase2 in the virus-producer cell (see Yoo et al.'s companion paper) may prevent activation of PR. According to this model, our observation that different retroviruses display differential requirements for nSMase2 activity suggests that either the lipid composition of these retroviruses differs or is differentially modulated by nSMase2, or that the rules that govern PR activation differ between the retroviruses that are sensitive or resistant to nSMase2 inhibition. Distinguishing among these possibilities will require further study.

By analyzing a series of Gag deletion mutants, we were able to exclude several domains of Gag as being required for the effect of nSMase2 disruption on HIV-1 Gag processing. Deletion of MA or p6, or replacement of NC with an Ile-zipper domain, did not alleviate the effect of PDDC or nSMase2-specific siRNA on Gag processing. These results suggest that a combination of domains, or the CA domain (which cannot be deleted in its entirety without abrogating particle assembly), may be responsible for the phenotype of nSMase2 disruption. Alternatively, as suggested above, the primary target of nSMase2 disruption could be activation of PR. In this context, it is important to note that PDDC itself is not a PR inhibitor, as determined by in vitro PR activity assays (see Yoo

et al.'s companion paper); we also observed the same effects on Gag processing with both PDDC and nSMase2 depletion, demonstrating that the observed phenotypes are not due to off-target effects of PDDC, which shows no significant interactions with other enzymes on the Eurofins safety 44-panel (47).

The effect of nSMase2 disruption on HIV-1 replication is distinct from that caused by manipulating cholesterol levels in cells and virions. Treatment of virus-producer cells with the cholesterol-chelating agent methyl-β-cyclodextrin, or inhibiting cholesterol biosynthesis with simvastatin, impaired particle production without interfering with Gag processing (17, 33). The inhibition of HIV-1 production from cholesterol-depleted cells was due to reduced Gag-membrane binding and impaired higher-order Gag multimerization (32). Similarly, treatment of virus-producer cells with the cholesterol-binding antifungal antibiotic amphotericin B methyl ester reduced HIV-1 release but did not induce a defect in Gag processing (78, 79). In contrast to the lack of an effect of nSMase2 disruption in target cells on HIV-1 infectivity, cholesterol depletion in target cells has been reported to impair particle infectivity (56, 57, 59). Thus, the effects of disrupting nSMase2 on HIV-1 replication are distinct from those imposed by cholesterol binding or depletion.

In conclusion, in this study, we demonstrate that inhibiting nSMase2 activity impairs the maturation of HIV-1 and other primate lentiviruses. Future work will extend these findings to obtain additional insights into the role of virion lipid composition in retroviral particle maturation. As described in more detail in the accompanying paper (Yoo et al. companion paper), nSMase2 may represent a unique target for therapeutic intervention in the HIV-1 replication cycle.

Methods

Cell Culture and Antibodies. HEK293T cells [obtained from the American Type Culture Collection (ATCC)], TZM-bl cells (obtained from J. C. Kappes through the NIH AIDS Reagent Program), and HeLa cells were maintained in Dulbecco's modified Eagle's medium (DMEM) containing 10 or 5% fetal bovine serum (FBS; HyClone), 2 mM glutamine, and 1% penicillin-streptomycin at 37 °C with 5% CO_2. HT1080 cells expressing murine ecotropic receptor mCAT-1 (HT1080-mCAT, a gift from A. Rein, NCI-Frederick, MD) were maintained in DMEM with 10% FBS, 2 mM glutamine, and 1% penicillin-streptomycin. Crandell–Rees feline kidney cells CRFK (a gift from S. Le Grice, NCI-Frederick, MD) were maintained in Eagle MEM supplemented with 10% FBS, 2 mM glutamine, and 1% penicillin-streptomycin. The SupT1 T cell line was cultured in Roswell Park Memorial Institute (RPMI) with 10% FBS and 1% penicillin-streptomycin. Primary hPBMCs were obtained from healthy volunteers from the NCI-Frederick Research Donor Program. The hPBMCs were extracted from whole blood using the Histopaque procedure (Sigma). Cells were then stimulated with phytohemagglutinin P (PHA-P) and IL-2 for 3 d. Anti-HIV-1 Ig, anti-HIV-1 p17, and anti-FIV p24Gag (clone PAK3-2C1) were obtained from the NIH AIDS Reagent Program. Reference immune serum from a naturally infected horse (Lady) (80) was a gift from R. Montelaro (University of Pittsburgh, Pittsburgh, PA). Anti-MLV p30 (CA) antibody was obtained from ViroMed Biosafety Laboratories. Anti-HIV PR was obtained from Abcam, and anti-HIV-1 p7 was a gift from R. Gorelick (NCI-Frederick, MD). Anti-A-MLV p15(E) Env antiserum was custom made in rabbits by Thermo Fisher Scientific using the peptide sequence C-RDSMALRERLNQRQKLFE. PDDC and compound 5 were synthesized as previously described (47) and were characterized by $^{1}H/^{13}C$ NMR for structural identification and confirmed to be of ≥95% purity by LC/MS. DPTIP and its inactive analog JHU3398 were synthesized as previously described (49).

Plasmids and Transfection. The following HIV-1 plasmids were used in this study: the full-length, infectious HIV-1 molecular clone pNL4-3 (81), and the mutant derivatives pNL4-3PR(−), which contains a point mutation in the PR active site (51); pNL4-3/Fyn(10)delMA (5, 32); pNL4-3-ILp1p6 (50); pNL4-3-p6L1Term (51); and pNL4-3ΔPolΔEnv (82). The subtype C transmitted/founder viral isolate K3016 (also known as CH185) (48) was a gift from Christina Ochsenbauer and John Kappes (University of Alabama, Birmingham, AL). The full-length SIV molecular clone SIVmac239 (83) was kindly provided by B. Crise and Y. Li (AIDS and Cancer Virus Program, NCI-Frederick). The full-length HIV-2 molecular clone HIV-2_{ROD10} was described previously (84) and was a gift from K. Strebel (NIAID, Bethesda). For EIAV Gag and GagPol expression, pCMV-EIAVuk was used [(85), a generous gift from R. Montelaro, University of Pittsburgh]. pSV-MLVψ−env− (86) was obtained from NIH AIDS Reagent Program. The FIV Orf2rep clone was described previously (87). The infectious MLV clone pRR390 (88) and the MLV vector expressing firefly luciferase, pRR460 (89), were gifts from A. Rein. One day after plating, the cells were transfected with the indicated plasmid DNA using Lipofectamine 2000 (Invitrogen) according to the manufacturer's recommendations. Six to eight hours posttransfection, the cells were treated with indicated concentrations of PDDC or inactive control compound in DMEM5. Virus-containing supernatants were filtered through a 0.45-μm membrane 24 or 48 h posttransfection; a portion was stored for infectivity assay, and the remainder was used to collect virus particles by ultracentrifugation. Virus pellets and cells were solubilized in lysis buffer [10 mM iodoacetamide (Sigma-Aldrich), complete PR inhibitor tablets (Roche), 300 mM sodium chloride, 50 mM Tris-HCl (pH 7.5), and 0.5% Triton X-100 (Sigma-Aldrich)] and used for further analysis. SupT1 cells were transfected with DEAE-dextran; 6 d later, the cells were divided into five equal parts and cultured in medium containing 0, 1, 3, 10 μM PDDC or 10 μM control compound in RPMI5 for another 48 h. The cells were spun down, the supernatant was filtered, the virus was pelleted, and cells and virus pellet were solubilized and used for western blotting. To monitor MLV particle infectivity, HEK293T cells were cotransfected with pRR390 and pBabeLuc; 6 to 8 h posttransfection, the cells were treated with indicated concentrations of PDDC or inactive control compound in DMEM5. Virus supernatant was collected 48 h posttransfection, filtered, and used for infectivity assay. For pseudotyping experiments, the pNL4-3/KFS clone was used, which expresses all HIV-1 proteins except Env (90), and A-MLV Env was expressed from pSV-A-MLVEnv (obtained through the NIH AIDS Reagent Program from N. Landau and D. Littman) (91).

siRNA-Mediated Knockdown of nSMase2. Lentiviral particles encoding siRNA specific for nSMase2 or scrambled siRNA (purchased from Applied Biological Materials) were used to transduce HEK293T or HeLa cells. One day after transduction, the cells were transfected with proviral molecular clones and fresh medium was added 6 to 8 h posttransfection. Virus supernatant was collected 24 or 48 h posttransfection, filtered, and used for further analysis.

Western Blotting. Cell and virus lysates were treated with 6x sodium dodecyl sulfate-polyacrylamide gel electrophoresis (SDS-PAGE) sample loading buffer [600 mM Tris-HCl (pH 6.8), 30% glycerol, 12% SDS, 20 mM dithiothreitol, 0.03% bromophenol blue] and heated at 95 °C for 5 min. Samples were analyzed on 4 to 15% Tris-glycine gels using a Bio-Rad Trans-Blot Turbo Transfer system according to the manufacturer's instructions. Proteins were detected with primary and secondary antibodies. Protein bands were visualized using chemiluminescence with Gel Doc XR+ system (Bio-Rad) and analyzed with Image Lab version 6.0.1 or AzureSpot (Azure Biosystems).

Single-Cycle Infectivity Assays. TZM-bl, a HeLa cell derivative harboring a stably integrated luciferase gene under transcriptional control of the HIV-1 long terminal repeat (LTR) (55), was infected with serial dilutions of virus stock in the presence of 20 μg/mL DEAE-dextran. Cells were lysed with BriteLite luciferase reagent (PerkinElmer), and luciferase was measured in a Wallac BetaMax plate reader at 48 h postinfection. Data were normalized to either untreated or scrambled siRNA-treated negative controls. MLV infectivity was measured in the HT1080mCAT1 cell line (92) 48 h after infection.

HIV-1 Replication. Virus replication kinetics were monitored in the SupT1 T cell line as previously described (78). Briefly, SupT1 cells were transfected with pNL4-3 (1 μg DNA/10^6 cells) in the presence of 700 μg/mL DEAE-dextran and were cultured in the absence and presence of 0.1, 0.3, or 1 μM of PDDC. The cells were split every 2 or 3 d with fresh medium containing or lacking PDDC. To monitor replication in PBMCs, NL4-3 virus was produced in HEK293T cells, normalized for RT activity, and used to inoculate stimulated (with 20 IU/mL human IL-2 and 5 mg/mL phytohemagglutinin from *Phaseolus vulgaris* for 48 h) hPBMCs. After a 2-h incubation, PBMCs were washed and resuspended in fresh RPMI5 containing 0, 0.1, 0.3, or 1 μM PDDC. Every 2 or 3 d, half the medium was replaced with

fresh medium without disturbing the cells. Virus replication was monitored by measuring the RT activity at each time point. RT activity values were plotted using GraphPad Prism to generate replication curves.

Thin-Section TEM. HEK293T cells were transfected with HIV-1, SIVmac, HIV-2, and MLV molecular clones, or CRFK cells were transfected with an FIV molecular clone, and 6 to 8 h posttransfection, cells were treated with or without PDDC at indicated concentrations. One day later, the cells were fixed with 2.5% glutaraldehyde and analyzed by TEM as described previously (93). Cell-free HIV-1 particles from SupT1 cells were pelleted by ultracentrifugation, fixed, and analyzed by TEM. For nSMase2 knockdown experiments, HEK293T cells were transduced with lentivirus particles containing nSMase2-specific or scrambled siRNA, and 24 h later transfected with HIV-1, SIVmac, HIV-2, or MLV molecular clones. One day later, the cells were fixed and processed for TEM as described above.

cryo-ET. To produce VLPs for cryo-ET analysis, HEK293T cells were seeded in 175-cm^2 flasks (nine flasks per particle preparation). One day after plating, the cells were transfected with pNL4-3ΔPolΔEnv plasmid using GeneJet transfection reagent (Ver. II) as per the manufacturer's recommendations. Eight hours posttransfection, the cells were replaced with DMEM containing 5 μM PDDC or without PDDC. Two days posttransfection, the virus supernatants were filtered through a 0.45-μm nitrocellulose membrane, and 35 mL of the supernatant was overlayed on 3 mL 8% OptiPrep in STE buffer. The virus was spun in an SW41 rotor at 100,000 × g for 1 h at 4 °C. The pellet was resuspended in PBS buffer and equilibrated on 30%, 20%, and 10% OptiPrep gradient for 2.5 h at 120,000 × g at 4 °C. The visible virus-containing fraction was collected, diluted 10 times in PBS, and spun at 160,000 × g for 80 min at 4 °C. The pellet was suspended in 30 μL of PBS and used for Cryo-ET analysis.

Cryo-ET tilt series were acquired using a Thermo Fisher Titan Krios operated at 300 keV equipped with a Gatan Quantum postcolumn energy filter (Gatan Inc.) operated in zero-loss mode with 20 eV slit width and a Gatan K3 direct electron detector in eBIC (Electron BioImaging Centre, Diamond). Tilt series were collected with SerialEM (94) with a nominal magnification of 64 k and a physical pixel size of 1.34 Å per pixel. They were acquired using a dose-symmetric tilt-scheme (95) starting from 0° with a 3° tilt increment by a group of three and an angular range of ±60°. The accumulated dose of each tilt series was around 123 $e^-/Å^2$ with a defocus range between −1.5 and −6 μm. In total, 45 tilt series from the control untreated sample and 43 tilt series from the PDDC-treated sample were collected. Each projection image was dose-fractioned into 10 frames. Details of data collection parameters are listed in *SI Appendix*, Table S1.

The automated cryoET pipeline developed in-house was used for initial tomograms (https://github.com/ffyr2w/cet_toolbox) through performing motion correction (96) of the raw frames, tilt-series alignment, and final reconstruction with IMOD (97). The fiducial markers were manually inspected to ensure the centering of predicted markers for each tilt series in eTOMO.

STA for both datasets was performed following the workflow of emClarity (60, 98). The in vitro assembled HIV-1 Gag structure (EMD-8403) (99) was low-pass filtered at 30 Å and was used as the initial template for template search in 6× binned tomograms with a pixel size of 8.06 Å. A total of 119,237 subtomograms were selected from 45 tilt series for the untreated dataset and 103,350 subtomograms were selected from 43 tilt series for the PDDC-treated dataset. The STA and alignment were performed iteratively using 6×, 5×, 4×, 3×, 2×, and 1× binned tomograms. A cylindrical alignment mask including seven hexamers and a sixfold symmetry was used throughout the alignment procedure. The final density maps were reconstructed at bin 1 and sharpened with a b-factor of −50.

Data, Materials, and Software Availability. Cryo-EM data have been deposited into the EM database. The accession numbers for untreated and PDDC-treated VLPs are EMD-15763 (100) and EMD-15764 (101), respectively.

ACKNOWLEDGMENTS. We thank members of the Freed lab for helpful discussion and critical review of the manuscript. We acknowledge the Diamond Light Source for access and support of the cryo-EM facilities at the UK National Electron Bioimaging Center (eBIC, proposal NT29812), funded by the Wellcome Trust, Media Research Center (MRC), and Biotechnology and Biological Sciences Research Council (BBSRC). Work in the Freed lab is supported by the Intramural Research Program of the Center for Cancer Research, National Cancer Institute, NIH. This work was additionally supported by the NIH P50 grant AI150481 (P.Z.), the UK Wellcome Trust Investigator Award 206422/Z/17/Z (P.Z.), the European Research Council AdG grant 101021133 (P.Z.), and the UK Biotechnology and Biological Sciences Research Council grant BB/S003339/1 (P.Z.). Work in the Haughey lab is supported by R01AG057420 (N.J.H. and B.S.S.) and R01MH131469 (N.J.H.), and the Slusher lab is supported by NIH grants R01 AG059799 and P30 MH075673 and a Maryland Innovation Initiative award (135726) from the Maryland Technology Development Corporation. We thank Clayton Smith and Ziqiu Wang, Center for Molecular Microscopy, NCI Advanced Technology Research Facility, Frederick, MD, for preparation and shipping of grids for cryo-ET studies.

Author affiliations: [a]Virus-Cell Interaction Section, HIV Dynamics and Replication Program, Center for Cancer Research, National Cancer Institute, Frederick, MD 21702; [b]Division of Structural Biology, Wellcome Trust Centre for Human Genetics, University of Oxford, Oxford OX3 7BN, United Kingdom; [c]Electron Microscopy Laboratory, Cancer Research Technology Program, Frederick National Laboratory for Cancer Research, Frederick, MD 21702; [d]Department of Neurology, Johns Hopkins University School of Medicine, Baltimore, MD 21287; [e]Electron Bio-Imaging Centre, Diamond Light Source, Harwell Science and Innovation Campus, Didcot OX11 0DE, United Kingdom; [f]Chinese Academy of Medical Sciences Oxford Institute, University of Oxford, Oxford OX3 7BN, United Kingdom; [g]Johns Hopkins Drug Discovery, Johns Hopkins University School of Medicine, Baltimore, MD 21287; and [h]Department of Psychiatry and Behavioral Sciences, Johns Hopkins University School of Medicine, Baltimore, MD 21287

1. E. O. Freed, HIV-1 assembly, release and maturation. *Nat. Rev. Microbiol.* **13**, 484–496 (2015).
2. A. B. Kleinpeter, E. O. Freed, HIV-1 maturation: Lessons learned from inhibitors. *Viruses* **12**, 940 (2020).
3. W. I. Sundquist, H. G. Krausslich, HIV-1 assembly, budding, and maturation. *Cold Spring Harb. Perspect. Med.* **2**, a006924 (2012).
4. F. Mucksch, V. Laketa, B. Muller, C. Schultz, H. G. Krausslich, Synchronized HIV assembly by tunable PIP2 changes reveals PIP2 requirement for stable Gag anchoring. *Elife* **6**, e25287 (2017).
5. A. Ono, S. D. Ablan, S. J. Lockett, K. Nagashima, E. O. Freed, Phosphatidylinositol (4,5) bisphosphate regulates HIV-1 Gag targeting to the plasma membrane. *Proc. Natl. Acad. Sci. U.S.A.* **101**, 14889–14894 (2004).
6. V. Chukkapalli, I. B. Hogue, V. Boyko, W. S. Hu, A. Ono, Interaction between the human immunodeficiency virus type 1 Gag matrix domain and phosphatidylinositol-(4,5)-bisphosphate is essential for efficient gag membrane binding. *J. Virol.* **82**, 2405–2417 (2008).
7. J. S. Saad *et al.*, Structural basis for targeting HIV-1 Gag proteins to the plasma membrane for virus assembly. *Proc. Natl. Acad. Sci. U.S.A.* **103**, 11364–11369 (2006).
8. L. A. Carlson *et al.*, Cryo electron tomography of native HIV-1 budding sites. *PLoS Pathog.* **6**, e1001173 (2010).
9. V. M. Vogt, Proteolytic processing and particle maturation. *Curr. Top. Microbiol. Immunol.* **214**, 95–131 (1996).
10. A. Wlodawer *et al.*, Conserved folding in retroviral proteases: Crystal structure of a synthetic HIV-1 protease. *Science* **245**, 616–621 (1989).
11. K. Qu *et al.*, Structure and architecture of immature and mature murine leukemia virus capsids. *Proc. Natl. Acad. Sci. U.S.A.* **115**, E11751–E11760 (2018).
12. M. Yeager, E. M. Wilson-Kubalek, S. G. Weiner, P. O. Brown, A. Rein, Supramolecular organization of immature and mature murine leukemia virus revealed by electron cryo-microscopy: Implications for retroviral assembly mechanisms. *Proc. Natl. Acad. Sci. U.S.A.* **95**, 7299–7304 (1998).
13. I. Katoh *et al.*, Murine leukemia virus maturation: Protease region required for conversion from "immature" to "mature" core form and for virus infectivity. *Virology* **145**, 280–292 (1985).
14. O. Pornillos, B. K. Ganser-Pornillos, Maturation of retroviruses. *Curr. Opin. Virol.* **36**, 47–55 (2019).
15. C. Favard *et al.*, HIV-1 Gag specifically restricts PI(4,5)P2 and cholesterol mobility in living cells creating a nanodomain platform for virus assembly. *Sci. Adv.* **5**, eaaw8651 (2019).
16. D. H. Nguyen, J. E. Hildreth, Evidence for budding of human immunodeficiency virus type 1 selectively from glycolipid-enriched membrane lipid rafts. *J. Virol.* **74**, 3264–3272 (2000).
17. A. Ono, E. O. Freed, Plasma membrane rafts play a critical role in HIV-1 assembly and release. *Proc. Natl. Acad. Sci. U.S.A.* **98**, 13925–13930 (2001).
18. P. Sengupta *et al.*, A lipid-based partitioning mechanism for selective incorporation of proteins into membranes of HIV particles. *Nat. Cell Biol.* **21**, 452–461 (2019).
19. P. Sengupta, J. Lippincott-Schwartz, Revisiting membrane microdomains and phase separation: A viral perspective. *Viruses* **12**, 745 (2020).
20. A. A. Waheed, E. O. Freed, The role of lipids in retrovirus replication. *Viruses* **2**, 1146–1180 (2010).
21. R. C. Aloia, F. C. Jensen, C. C. Curtain, P. W. Mobley, L. M. Gordon, Lipid composition and fluidity of the human immunodeficiency virus. *Proc. Natl. Acad. Sci. U.S.A.* **85**, 900–904 (1988).
22. R. C. Aloia, H. Tian, F. C. Jensen, Lipid composition and fluidity of the human immunodeficiency virus envelope and host cell plasma membranes. *Proc. Natl. Acad. Sci. U.S.A.* **90**, 5181–5185 (1993).
23. B. Brugger *et al.*, The HIV lipidome: A raft with an unusual composition. *Proc. Natl. Acad. Sci. U.S.A.* **103**, 2641–2646 (2006).
24. R. Chan *et al.*, Retroviruses human immunodeficiency virus and murine leukemia virus are enriched in phosphoinositides. *J. Virol.* **82**, 11228–11238 (2008).
25. M. Lorizate *et al.*, Probing HIV-1 membrane liquid order by Laurdan staining reveals producer cell-dependent differences. *J. Biol. Chem.* **284**, 22238–22247 (2009).
26. M. Lorizate *et al.*, Comparative lipidomics analysis of HIV-1 particles and their producer cell membrane in different cell lines. *Cell Microbiol.* **15**, 292–304 (2013).

27. J. E. Pessin, M. Glaser, Budding of Rous sarcoma virus and vesicular stomatitis virus from localized lipid regions in the plasma membrane of chicken embryo fibroblasts. *J. Biol. Chem.* **255**, 9044–9050 (1980).
28. L. Ding, A. Derdowski, J. J. Wang, P. Spearman, Independent segregation of human immunodeficiency virus type 1 Gag protein complexes and lipid rafts. *J. Virol.* **77**, 1916–1926 (2003).
29. R. Halwani, A. Khorchid, S. Cen, L. Kleiman, Rapid localization of Gag/GagPol complexes to detergent-resistant membrane during the assembly of human immunodeficiency virus type 1. *J. Virol.* **77**, 3973–3984 (2003).
30. K. Holm, K. Weclewicz, R. Hewson, M. Suomalainen, Human immunodeficiency virus type 1 assembly and lipid rafts: Pr55(gag) associates with membrane domains that are largely resistant to Brij98 but sensitive to Triton X-100. *J. Virol.* **77**, 4805–4817 (2003).
31. O. W. Lindwasser, M. D. Resh, Multimerization of human immunodeficiency virus type 1 Gag promotes its localization to barges, raft-like membrane microdomains. *J. Virol.* **75**, 7913–7924 (2001).
32. A. Ono, A. A. Waheed, E. O. Freed, Depletion of cellular cholesterol inhibits membrane binding and higher-order multimerization of human immunodeficiency virus type 1 Gag. *Virology* **360**, 27–35 (2007).
33. W. F. Pickl, F. X. Pimentel-Muinos, B. Seed, Lipid rafts and pseudotyping. *J. Virol.* **75**, 7175–7183 (2001).
34. C. Beer, L. Pedersen, Amphotropic murine leukemia virus is preferentially attached to cholesterol-rich microdomains after binding to mouse fibroblasts. *Virol. J.* **3**, 21 (2006).
35. X. Feng, N. V. Heyden, L. Ratner, Alpha interferon inhibits human T-cell leukemia virus type 1 assembly by preventing Gag interaction with rafts. *J. Virol.* **77**, 13389–13395 (2003).
36. A. Ono, A. A. Waheed, A. Joshi, E. O. Freed, Association of human immunodeficiency virus type 1 gag with membrane does not require highly basic sequences in the nucleocapsid: Use of a novel Gag multimerization assay. *J. Virol.* **79**, 14131–14140 (2005).
37. S. Campbell *et al.*, The raft-promoting property of virion-associated cholesterol, but not the presence of virion-associated Brij 98 rafts, is a determinant of human immunodeficiency virus type 1 infectivity. *J. Virol.* **78**, 10556–10565 (2004).
38. S. M. Campbell, S. M. Crowe, J. Mak, Virion-associated cholesterol is critical for the maintenance of HIV-1 structure and infectivity. *AIDS* **16**, 2253–2261 (2002).
39. D. R. Graham, E. Chertova, J. M. Hilburn, L. O. Arthur, J. E. Hildreth, Cholesterol depletion of human immunodeficiency virus type 1 and simian immunodeficiency virus with beta-cyclodextrin inactivates and permeabilizes the virions: Evidence for virion-associated lipid rafts. *J. Virol.* **77**, 8237–8248 (2003).
40. A. A. Shamseddine, M. V. Airola, Y. A. Hannun, Roles and regulation of neutral sphingomyelinase-2 in cellular and pathological processes. *Adv. Biol. Regul.* **57**, 24–41 (2015).
41. N. Bartke, Y. A. Hannun, Bioactive sphingolipids: Metabolism and function. *J. Lipid. Res.* **50**, S91–S96 (2009).
42. Y. A. Hannun, L. M. Obeid, Many ceramides. *J. Biol. Chem.* **286**, 27855–27862 (2011).
43. D. Haubert *et al.*, PtdIns(4,5)P-restricted plasma membrane localization of FAN is involved in TNF-induced actin reorganization. *EMBO J.* **26**, 3308–3321 (2007).
44. S. Philipp *et al.*, The Polycomb group protein EED couples TNF receptor 1 to neutral sphingomyelinase. *Proc. Natl. Acad. Sci. U.S.A.* **107**, 1112–1117 (2010).
45. C. M. Finnegan *et al.*, Ceramide, a target for antiretroviral therapy. *Proc. Natl. Acad. Sci. U.S.A.* **101**, 15452–15457 (2004).
46. E. Barklis *et al.*, Ceramide synthase 2 deletion decreases the infectivity of HIV-1. *J. Biol. Chem.* **296**, 100340 (2021).
47. C. Rojas *et al.*, A novel and potent brain penetrant inhibitor of extracellular vesicle release. *Br. J. Pharmacol.* **176**, 3857–3870 (2019).
48. N. F. Parrish *et al.*, Phenotypic properties of transmitted founder HIV-1. *Proc. Natl. Acad. Sci. U.S.A.* **110**, 6626–6633 (2013).
49. C. Rojas *et al.*, DPTIP, a newly identified potent brain penetrant neutral sphingomyelinase 2 inhibitor, regulates astrocyte-peripheral immune communication following brain inflammation. *Sci. Rep.* **8**, 17715 (2018).
50. M. A. Accola, B. Strack, H. G. Gottlinger, Efficient particle production by minimal Gag constructs which retain the carboxy-terminal domain of human immunodeficiency virus type 1 capsid-p2 and a late assembly domain. *J. Virol.* **74**, 5395–5402 (2000).
51. M. Huang, J. M. Orenstein, M. A. Martin, E. O. Freed, p6Gag is required for particle production from full-length human immunodeficiency virus type 1 molecular clones expressing protease. *J. Virol.* **69**, 6810–6818 (1995).
52. L. E. Henderson, R. Sowder, T. D. Copeland, G. Smythers, S. Oroszlan, Quantitative separation of murine leukemia virus proteins by reversed-phase high-pressure liquid chromatography reveals newly described gag and env cleavage products. *J. Virol.* **52**, 492–500 (1984).
53. A. Rein, J. Mirro, J. G. Haynes, S. M. Ernst, K. Nagashima, Function of the cytoplasmic domain of a retroviral transmembrane protein: p15E–p2E cleavage activates the membrane fusion capability of the murine leukemia virus Env protein. *J. Virol.* **68**, 1773–1781 (1994).
54. R. E. Kiernan, E. O. Freed, Cleavage of the murine leukemia virus transmembrane env protein by human immunodeficiency virus type 1 protease: Transdominant inhibition by matrix mutations. *J. Virol.* **72**, 9621–9627 (1998).
55. E. J. Platt, K. Wehrly, S. E. Kuhmann, B. Chesebro, D. Kabat, Effects of CCR5 and CD4 cell surface concentrations on infections by macrophagetropic isolates of human immunodeficiency virus type 1. *J. Virol.* **72**, 2855–2864 (1998).
56. Z. Liao, L. M. Cimakasky, R. Hampton, D. H. Nguyen, J. E. Hildreth, Lipid rafts and HIV pathogenesis: Host membrane cholesterol is required for infection by HIV type 1. *AIDS Res. Hum. Retroviruses* **17**, 1009–1019 (2001).
57. S. Manes *et al.*, Membrane raft microdomains mediate lateral assemblies required for HIV-1 infection. *EMBO Rep.* **1**, 190–196 (2000).
58. D. H. Nguyen, D. D. Taub, Inhibition of chemokine receptor function by membrane cholesterol oxidation. *Exp. Cell Res.* **291**, 36–45 (2003).
59. W. Popik, T. M. Alce, W. C. Au, Human immunodeficiency virus type 1 uses lipid raft-colocalized CD4 and chemokine receptors for productive entry into CD4(+) T cells *J. Virol.* **76**, 4709–4722 (2002).
60. B. A. Himes, P. Zhang, emClarity: Software for high-resolution cryo-electron tomography and subtomogram averaging. *Nat. Methods* **15**, 955–961 (2018).
61. R. A. Dick, D. L. Mallery, V. M. Vogt, L. C. James, IP6 regulation of HIV capsid assembly, stability, and uncoating. *Viruses* **10**, 640 (2018).
62. S. K. Lee *et al.*, Context surrounding processing sites is crucial in determining cleavage rate of a subset of processing sites in HIV-1 Gag and Gag-Pro-Pol polyprotein precursors by viral protease. *J. Biol. Chem.* **287**, 13279–13290 (2012).
63. J. Harrison *et al.*, Cryo-EM structure of the HIV-1 Pol polyprotein provides insights into virion maturation. *Sci. Adv.* **8**, eabn9874 (2022).
64. J. Agniswamy, J. M. Sayer, I. T. Weber, J. M. Louis, Terminal interface conformations modulate dimer stability prior to amino terminal autoprocessing of HIV-1 protease. *Biochemistry* **51**, 1041–1050 (2012).
65. J. M. Louis, G. M. Clore, A. M. Gronenborn, Autoprocessing of HIV-1 protease is tightly coupled to protein folding. *Nat. Struct. Biol.* **6**, 868–875 (1999).
66. S. J. Arrigo, K. Huffman, Potent inhibition of human immunodeficiency virus type 1 (HIV-1) replication by inducible expression of HIV-1 PR multimers. *J. Virol.* **69**, 5988–5994 (1995).
67. V. Karacostas, E. J. Wolffe, K. Nagashima, M. A. Gonda, B. Moss, Overexpression of the HIV-1 gag-pol polyprotein results in intracellular activation of HIV-1 protease and inhibition of assembly and budding of virus-like particles. *Virology* **193**, 661–671 (1993).
68. H. G. Krausslich, Human immunodeficiency virus proteinase dimer as component of the viral polyprotein prevents particle assembly and viral infectivity. *Proc. Natl. Acad. Sci. U.S.A.* **88**, 3213–3217 (1991).
69. J. Park, C. D. Morrow, Overexpression of the gag-pol precursor from human immunodeficiency virus type 1 proviral genomes results in efficient proteolytic processing in the absence of virion production. *J. Virol.* **65**, 5111–5117 (1991).
70. A. H. Kaplan *et al.*, Partial inhibition of the human immunodeficiency virus type 1 protease results in aberrant virus assembly and the formation of noninfectious particles. *J. Virol.* **67**, 4050–4055 (1993).
71. H. G. Krausslich, Specific inhibitor of human immunodeficiency virus proteinase prevents the cytotoxic effects of a single-chain proteinase dimer and restores particle formation. *J. Virol.* **66**, 567–572 (1992).
72. M. D. Moore *et al.*, Suboptimal inhibition of protease activity in human immunodeficiency virus type 1: Effects on virion morphogenesis and RNA maturation. *Virology* **379**, 152–160 (2008).
73. B. Muller *et al.*, HIV-1 Gag processing intermediates trans-dominantly interfere with HIV-1 infectivity. *J. Biol. Chem.* **284**, 29692–29703 (2009).
74. K. Wiegers *et al.*, Sequential steps in human immunodeficiency virus particle maturation revealed by alterations of individual Gag polyprotein cleavage sites. *J. Virol.* **72**, 2846–2854 (1998).
75. A. H. Kaplan, M. Manchester, R. Swanstrom, The activity of the protease of human immunodeficiency virus type 1 is initiated at the membrane of infected cells before the release of viral proteins and is required for release to occur with maximum efficiency. *J. Virol.* **68**, 6782–6786 (1994).
76. J. Schimer *et al.*, Triggering HIV polyprotein processing by light using rapid photodegradation of a tight-binding protease inhibitor. *Nat. Commun.* **6**, 6461 (2015).
77. C. O. Tabler *et al.*, The HIV-1 viral protease is activated during assembly and budding prior to particle release. *J. Virol.* **96**, e0219821 (2022).
78. A. A. Waheed *et al.*, Inhibition of HIV-1 replication by amphotericin B methyl ester: Selection for resistant variants. *J. Biol. Chem.* **281**, 28699–28711 (2006).
79. A. A. Waheed *et al.*, Inhibition of human immunodeficiency virus type 1 assembly and release by the cholesterol-binding compound amphotericin B methyl ester: Evidence for Vpu dependence. *J. Virol.* **82**, 9776–9781 (2008).
80. R. C. Montelaro, B. Parekh, A. Orrego, C. J. Issel, Antigenic variation during persistent infection by equine infectious anemia virus, a retrovirus. *J. Biol. Chem.* **259**, 10539–10544 (1984).
81. A. Adachi *et al.*, Production of acquired immunodeficiency syndrome-associated retrovirus in human and nonhuman cells transfected with an infectious molecular clone. *J. Virol.* **59**, 284–291 (1986).
82. S. B. Van Engelenburg *et al.*, Distribution of ESCRT machinery at HIV assembly sites reveals virus scaffolding of ESCRT subunits. *Science* **343**, 653–656 (2014).
83. D. A. Regier, R. C. Desrosiers, The complete nucleotide sequence of a pathogenic molecular clone of simian immunodeficiency virus. *AIDS Res. Hum. Retroviruses* **6**, 1221–1231 (1990).
84. M. A. Ryan-Graham, K. W. Peden, Both virus and host components are important for the manifestation of a Nef- phenotype in HIV-1 and HIV-2. *Virology* **213**, 158–168 (1995).
85. C. Chen, F. Li, R. C. Montelaro, Functional roles of equine infectious anemia virus Gag p9 in viral budding and infection. *J. Virol.* **75**, 9762–9770 (2001).
86. N. R. Landau, D. R. Littman, Packaging system for rapid production of murine leukemia virus vectors with variable tropism. *J. Virol.* **66**, 5110–5113 (1992).
87. A. K. Waters *et al.*, Influence of ORF2 on host cell tropism of feline immunodeficiency virus. *Virology* **215**, 10–16 (1996).
88. A. Rein, M. R. McClure, N. R. Rice, R. B. Luftig, A. M. Schultz, Myristylation site in Pr65gag is essential for virus particle formation by Moloney murine leukemia virus. *Proc. Natl. Acad. Sci. U.S.A.* **83**, 7246–7250 (1986).
89. J. P. Morgenstern, H. Land, Advanced mammalian gene transfer: High titre retroviral vectors with multiple drug selection markers and a complementary helper-free packaging cell line. *Nucleic Acids Res.* **18**, 3587–3596 (1990).
90. E. O. Freed, E. L. Delwart, G. L. Buchschacher Jr., A. T. Panganiban, A mutation in the human immunodeficiency virus type 1 transmembrane glycoprotein gp41 dominantly interferes with fusion and infectivity. *Proc. Natl. Acad. Sci. U.S.A.* **89**, 70–74 (1992).
91. N. R. Landau, K. A. Page, D. R. Littman, Pseudotyping with human T-cell leukemia virus type I broadens the human immunodeficiency virus host range. *J. Virol.* **65**, 162–169 (1991).
92. Y. S. Ahi *et al.*, Functional interplay between murine leukemia virus Glycogag, Serinc5, and surface glycoprotein governs virus entry, with opposite effects on gammaretroviral and ebolavirus glycoproteins. *mBio* **7**, e01985–16 (2016).
93. E. O. Freed, J. M. Orenstein, A. J. Buckler-White, M. A. Martin, Single amino acid changes in the human immunodeficiency virus type 1 matrix protein block virus particle production. *J. Virol.* **68**, 5311–5320 (1994).
94. D. N. Mastronarde, Automated electron microscope tomography using robust prediction of specimen movements. *J. Struct. Biol.* **152**, 36–51 (2005).
95. W. J. H. Hagen, W. Wan, J. A. G. Briggs, Implementation of a cryo-electron tomography tilt-scheme optimized for high resolution subtomogram averaging. *J. Struct. Biol.* **197**, 191–198 (2017).
96. S. Q. Zheng *et al.*, MotionCor2: Anisotropic correction of beam-induced motion for improved cryo-electron microscopy. *Nat. Methods* **14**, 331–332 (2017).
97. D. N. Mastronarde, S. R. Held, Automated tilt series alignment and tomographic reconstruction in IMOD. *J. Struct. Biol.* **197**, 102–113 (2017).
98. T. Ni *et al.*, High-resolution in situ structure determination by cryo-electron tomography and subtomogram averaging using emClarity. *Nat. Protoc.* **17**, 421–444 (2022).
99. J. Ning *et al.*, In vitro protease cleavage and computer simulations reveal the HIV-1 capsid maturation pathway. *Nat. Commun.* **7**, 13689 (2016).
100. A. A. Waheed *et al.*, Untreatment WT HIV-1 immature gag. *Electron Microscopy Data Bank*. https://www.ebi.ac.uk/emdb/EMD-15763. Deposited 6 September 2022.
101. A. A. Waheed *et al.*, PDDC treatment HIV immature Gag. *Electron Microscopy Data Bank*. https://www.ebi.ac.uk/emdb/EMD-15764. Deposited 6 September 2022.